Article

Self-Micellizing Solid Dispersion of Thymoquinone with Enhanced Biopharmaceutical and Nephroprotective Effects

Shimul Halder[1*], Sanjida Afrose[1#], Manik Chandra Shill[2#], Nahid Sharmin[1], Patricia Prova Mollick [2], Madhabi Lata Shuma[3], Md. Abdul Muhit[4] and S. M. Abdur Rahman[4]

[1]Department of Pharmaceutical Technology, Faculty of Pharmacy, University of Dhaka, Dhaka-1000, Bangladesh.
[2]Department of Pharmaceutical Sciences, North South University, Dhaka-1229, Bangladesh.
[3]Department of Pharmacy, Stamford University Bangladesh, Siddeswari Dhaka-1217, Bangladesh.
[4]Department of Clinical Pharmacy and Pharmacology, Faculty of Pharmacy, University of Dhaka, Dhaka 1000, Bangladesh.
* Correspondence: author: shimulpht@du.ac.bd
#, equal contribution

ABSTRACT

Nigella sativa's thymoquinone (TQM), a water-insoluble phytonutrient exhibits nephroprotective effects. This study intends to develop a self-micellizing solid dispersion (SMSD) of TQM for better biopharmaceutical and nephroprotective performance. Soluplus®-based SMSD of TQM was created and tested for physicochemical properties, solubility, and pharmacokinetics in rats. Plasma creatinine, blood urea nitrogen (BUN), nephrotoxic indicators, and oxidative stress biomarkers were also tested. During SMSD preparation, TQM was found amorphous, boosting solubility. Minimal band changes between TQM and Soluplus® indicate insignificant drug-carrier interactions. SMSD-TQM generated fine micelles in water, improving TQM's solubility by 97.8% in 60 min. SMSD-TQM was 4.9 times more bioavailable orally in rats than crystalline TQM. In a rat model of acute renal damage by cisplatin (6 mg/kg, *i.p.*), SMSD-TQM (10 mg-TQM/kg, *p.o.*) reduced blood creatinine and BUN by 56% and 63.2%, respectively. These findings imply that SMSD-TQM may be a potent dosage option for enhancing TQM's nutrient value.

Keywords: biopharmaceutical; nephroprotective; oral absorption; self-micellizing solid dispersion; thymoquinone

 doi:10.20944/preprints202211.0372.v1

1. Introduction

Noncommunicable diseases, in particular, hypertension and kidney disease remain a major contributor to the morbidity and mortality throughout the world (Dera et al., 2020). Chronic kidney disease (CKD) is a major public health concern with an overall prevalence in Bangladeshi people of 22.48% which was higher than the global prevalence of CKD (Banik & Ghosh, 2021). Thymoquinone (TQM) is one of the most pharmacologically active constituent obtained from Black Cumin seeds (*Nigella sativa*), which is widely used in traditional medicine as a holistic treatment option (Goyal et al., 2017). TQM possesses anticancer, antischistosomal, antifungal, antibacterial, anticonvulsant, hepatoprotective, and neuroprotective activities (Shaterzadeh-Yazdi et al., 2018). In addition, the drug exerts its nephroprotective effects through anti-inflammatory and antioxidant activities (Farooqui et al., 2017). However, poor aqueous solubility and the consequent inferior oral bioavailability of the drug limits its clinical effect (Elmowafy et al., 2016). Solubility of TQM in water was reported <1.0 mg/mL at room temperature and therefore high doses are required in clinical application as a nutraceutical agent (Fahmy et al., 2020). Improvement of the dissolution behavior of TQM can enhance oral bioavailability, which, in turn, may increase the therapeutic efficiency of TQM. Very few studies have been reported targeting to improve the therapeutic potential of TQM including micelle nanoparticles, chitosan nanoparticles, liposomes, suspension, and solution formulations. Although these oral liquid formulations enhanced the solubility and bioavailability of TQM, drugs in these formulations were more prone to degradation than solid state. These observations prompted us to develop a solid formulation of TQM with high stability, while ensuring an improved dissolution behavior and oral bioavailability.

The solubility of a poorly water soluble drug can be enhanced by employing various formulation strategies such as employment of a surfactant, pH modification, nano-suspension

 doi:10.20944/preprints202211.0372.v1

technology, hydrotrophy, solid dispersion, and salt formation. However, among these techniques, Solid dispersion (SD) technology is widely used to increase the water solubility, dissolution rate, and bioavailability of the drugs with poor water-solubility (Sareen et al., 2012). SD involves the molecular dispersion of one or more APIs in an inert hydrophilic carrier, which helps to improve the solubility of the drug (Alam et al., 2012). The solid state of drugs in the solid dispersions can be amorphous and/or crystalline. When the drug is in the amorphous state, it can be incorporated in the solid dispersion as particles or dispersed over the carrier at a molecular level (Benzoate, 2019; Fahr & Liu, 2007). However, when the drug is in the crystalline state, it is incorporated as particles only where it can form mixed crystals with the carrier (Chavan et al., 2016). However, to our knowledge, such mixed crystals have never been encountered with solid dispersions.

Recently another promising formulation approach self-micellizing solid dispersion (SMSD), has drawn noticeable attention as it can improve the bioavailability of drugs as well as restrain the consistency in oral absorption under different patho-physiological conditions (Onoue, Yamada, et al., 2014). SMSD technology is a solid dispersion system with the use of an amphiphilic block co-polymer which can achieve high dissolution characteristics of poorly water soluble compounds by its self-micellizing potency (Kojo et al., 2017a; Onoue, Suzuki, et al., 2014a; Suzuki, Kojo, et al., 2016; Suzuki, Sato, et al., 2016). An amphiphilic polymer consists of a hydrophobic unit and a hydrophilic unit; and the self–micelleization by the polymer occurs with encapsulation of a lipophilic drug through hydrophobic interaction when introduced in dissolution media (Letchford & Burt, 2007). Therefore, SMSD system might be beneficial to improve the biopharmaceutical properties of TQM and enhance the nephroprotective effects even at a lower dose. However little is known about the feasibility of SMSD system incorporating TQM in ameliorating the nephroprotective properties.

 doi:10.20944/preprints202211.0372.v1

The present study aims to develop a self-micellizing solid dispersion (SMSD) formulation of TQM (SMSD-TQM) employing an amphiphilic polymer with the objective of enhanced biopharmaceutical and improved nephroprotective function. The developed formulations were examined for the physicochemical properties, particle size distribution, morphology, crystallinity, and dissolution behavior. Pharmacokinetics of TQM was also evaluated in rats after oral administration of TQM and SMSD-TQM. Finally, the nephroprotective effects of TQM samples were investigated in cisplatin induced acute kidney injury rat models.

Preprints (www.preprints.org) | NOT PEER-REVIEWED | Posted: 21 November 2022 doi:10.20944/preprints202211.0372.v1

2. Materials and Methods

2.1 Materials

TQM was purchased from Sigma-Aldrich (USA). BASF, Dhaka, Bangladesh kindly donated Soluplus®, Kolliphor® P188, and Kolliphor® P407. All other chemicals and reagents were purchased commercially.

2.2 Standard Curve Preparation and TQM Content Analysis

By dissolving 10 mg of TQM with enough methanol in a volumetric flask to achieve a final concentration of 1 mg/mL, a 10 mL stock solution of TQM was created. The Beer-Lambert equation is followed by TQM in the concentration range of 8 to 30 µg/mL, and TQM provides a suitable absorbance value at 257 nm. (Noor et al., 2021). Therefore, the stock solutions were then diluted sequentially at various concentrations prior to use and the corresponding absorbance were determined at 257 nm using a UV-vis spectrophotometer (UV-1800, Shimadzu Corporation, Japan). Using the equation derived from the standard curve, the amount of TQM was determined.

2.3 Phase Solubility Study

To select an appropriate carrier, the apparent solubility of TQM in polymer solutions was assessed in triplicate using a proven method established by Higuchi and Connors. (Higuchi, T and Connors, 1965).

An excess of TQM (about 1 gm) was added to the aqueous solutions of Soluplus®, Kolliphor® P188, and Kolliphor® P407 at a polymer concentration of 2–25 mg/mL. The tubes were then sealed and shaken for 48 hours at 75 rpm at 37°C in a thermostatically controlled water bath (WBS-C1, Wincom, China). The suspension that resulted was centrifuged at 10,000×*g* for 10 min after 48 hours, and the supernatant was filtered. The resultant

Preprints (www.preprints.org) | NOT PEER-REVIEWED | Posted: 21 November 2022 doi:10.20944/preprints202211.0372.v1

supernatants were then filtered, and the approach stated in the preceding section was used to determine the TQM content.

The stability constant (Ks) and complexation efficiency (C.E.) were calculated using the equations below;

$$Ks = \frac{slope}{So\ (1-slope)}$$

$$C.E. = \frac{slope}{(1-slope)}$$

Where, S_o is the equilibrium aqueous solubility of TQM, and the slope is attained by plotting TQM concentration versus different polymer concentrations.

2.4 Preparation of SMSD-TQM

The SMSD-TQM was prepared via a solvent evaporation process. In the selection step of the polymer ratio, crystalline TQM and a chosen polymer were dissolved in methanol based on their apparent solubility and complexation behavior. The solution was then dried using a rotary vacuum-dryer (RVD) (Heidolph Rota-Vap, Germany). The freeze-drying (FD) procedure was also used in the preparation of SMSD-TQM in order to compare the impact of drying on the physicochemical behavior of the approach. Accurately weighed crystalline TQM (10% w/w) and polymer were dissolved in 1, 4-dioxane and then frozen at -80°C. The frozen samples were subsequently lyophilized using an Eyela FD-1000 freeze dryer for 24 h at a pressure of 15 Pa. (Tokyo Rikakikai, Tokyo, Japan).

2.5 Dissolution Study

To provide insight into the enhanced release of TQM over time, the in vitro dissolution test on TQM samples was carried out under non-sink conditions. The dissolution investigation was conducted in 50 mL of distilled water at 37±0.5 °C with continuous stirring of 50 rpm by a magnetic stirrer for 60 min. At regular intervals, samples (1 mL) were

Preprints (www.preprints.org) | NOT PEER-REVIEWED | Posted: 21 November 2022 doi:10.20944/preprints202211.0372.v1

withdrawn and centrifuged at 10,000×*g* for 5 min before being filtered through a 0.45 μm membrane filter and having the supernatant diluted with 50% methanol. At 257 nm, the amount of TQM in the media was measured spectrophotometrically.

2.6 Surface Morphology

Scanning electron microscopy (SEM) method was used to study the surface morphology of TQM samples (JEOL JSM-7600F, Tokyo, Japan). Double-sided carbon tape was used to secure the samples to an aluminum sample holder before a magnetron sputtering apparatus was used to cover the samples with platinum.

2.7 X-ray Powder Diffraction (XRPD)

Using a Mini Flex II (Rigaku, Tokyo, Japan), XRPD patterns of TQM samples were captured using Cu Kα radiation produced at 40 mA and 35 kV. Samples were scanned at a speed of 4°/min and a step size of 0.2° over a range of 2 angles from 10° to 35°.

2.8 Differential Scanning Calorimetry (DSC)

A Simultaneous Thermal Analyzer (NETZSCH STA 449F5TA Instruments, USA) was used to measure the thermal behavior of TQM samples. The samples (3 mg) were heated at a rate of 5°C/min while purging the sample with nitrogen gas (50 mL/min). Indium was used as the calibration standard (8–10 mg, 99.999% pure, onset at 156.6°C).

2.9 Dynamic Light Scattering (DLS)

A Zetasizer was used to evaluate the average particle size and Zeta potential of SMSD-TQM samples that were suspended in water using the DLS method (MALVERN,

Preprints (www.preprints.org) | NOT PEER-REVIEWED | Posted: 21 November 2022 doi:10.20944/preprints202211.0372.v1

Worcestershire, UK). All measurements were made at 25°C and a measurement angle of 90°, and the mean diameter was estimated using photon correlation from light scattering..

2.10 Transmission Electron Microscopy (TEM)

10 mg TQM equivalent SMSD-TQM was dissolved in 1 mL of distilled water for the TEM experiment, and an aliquot (5 µL) was spread out on a 200 mesh copper grid that had been covered with carbon. The sample was left to stand for 60 seconds before any extra solution was blotted away. The samples were then visualized under a high-resolution transmission electron microscope (F200X Talos, Thermo Fisher, Waltham, MA, USA) operating at 200 kV.

2.11 Fourier Transform Infrared Spectroscopy (FT-IR)

The compatibility and any potential interactions between the SMSD-TQM components were evaluated using FT-IR analysis. The samples were individually placed on the sample platform of the instrument (Shimadzu, IR Spirit, Japan), and IR spectra were acquired using LC Solution software in the range of 4000–600 cm^{-1}. For each sample, the baseline was normalized and corrected during the analysis.

2.12 Animals

Male Wister rats weighing 220±24 g (8-9 weeks old) were chosen in the animal experiment. They were kept in a laboratory setting with free access to food and water. The Faculty of Biological Sciences at the University of Dhaka's institutional Animal Care and Ethical Committee gave its approval for the study's procedures (approval number 111).

2.13 Pharmacokinetic Studies

Preprints (www.preprints.org) | NOT PEER-REVIEWED | Posted: 21 November 2022 doi:10.20944/preprints202211.0372.v1

Prior to administering TQM samples, experimental rats were fasted for the previous night while still being given free access to water. The dose for crystalline TQM was made with a 0.25% suspension of carboxy methyl cellulose (CMC). With distilled water, SMSD-TQM dispersion was made. Unanesthetized rats' tail veins were used to collect 300 µL of heparinized blood samples at the specified time intervals of 0.25, 0.5, 1, 2, 4, and 6 h. The blood samples were then centrifuged at 10,000×*g* for 10 min, and 400 µL of acetonitrile and an internal standard (diclofenac at a fixed concentration of 10 µg/mL) were added. The mixture was then kept in an ice bath for one minute before being vortexed for one minute again kept on ice bath for an additional time. The samples were then centrifuged for 5 minutes at 3,000× *g*.

The filtrate was then analyzed by an internal standard method using a Shimadzu HPLC system composed of a SCL-20Avp system controller, an LC-20AD vp solvent delivery pump, a DGU-14A degasser, a CTO-20A vp column oven, and an SPD-20A Prominence UV-vis detector. Binary gradient mobile phase made up of Milli-Q (A) and methanol (B) delivered at a flow rate of 1.0 mL/min was used in a Phenomenex, reversed-phase C18, 150 mm×4.6 mm, 5 µm column maintained at 35°C.

The mobile phase's gradient condition was as follows: 85% B for the first 20 minutes; 85-95% B for the next 5 minutes; 95-85% B for the next 5 minutes; and 85% B for the last 5 minutes. Pharmacokinetic parameters were then calculated by means of non-compartmental models using PK solver (an add-on program in Microsoft excel) (Y. Zhang et al., 2010).

2.14 Nephroprotective Effect of TQM Samples

2.14.1 Rat Model of Nephropathy

The nephrotoxic potential of TQM in rats was assessed using an animal model of nephropathy induced by cisplatin, as previously reported (Choie et al., 1981). A rat model of

Preprints (www.preprints.org) | NOT PEER-REVIEWED | Posted: 21 November 2022 doi:10.20944/preprints202211.0372.v1

nephropathy was prepared by intraperitoneal administration of cisplatin (6 mg/kg) dissolved in saline, and as a control experiment, saline was injected. TQM samples (10 mg/kg) were dissolved in 1 mL of distilled water and administered orally to rats at 24 h before to 72 h after cisplatin treatment repeating every 24 h. Following the oral administration of TQM samples, blood was drawn at 76 h and plasma was then obtained by centrifuging the blood at 10,000×*g* for 10 minutes to obtain several biomarkers of nephropathy. Until analysis, plasma samples were stored frozen at -80°C.

2.14.2 Blood Urea Nitrogen (BUN)

BUN level was measured as reported previously (Sampson & Baird, 1979). Briefly, solution 1 containing 2 IU/mL GLDH, 0.27 mg/mL NADPH・4Na and 1.5 mg/mL *α*-KG (160 μL) and solution 2 containing 9 IU/mL urease and 1.5 mg/mL *α*-KG (40 μL) were added to the plasma sample (2.7 μL), followed by incubation in the 96-well microplate at room temperature for 10 min. After the incubation, measure the absorbance of sample at 340 nm with the blank solution as the control using SAFIRE (TECHAN, Männedorf, Swizerland).

2.14.3 Creatinine

Plasma creatinine level was measured as reported previously (Nihei et al., 2021). The plasma sample (50 μL) was incubated with a deproteinizing solution comprising sodium tungstate and phosphoric acid (300 μL) for 10 minutes before being centrifuged at 2,500×*g* for 10 minutes. The supernatant (100 μL) was collected for mixing with 22 mmol/L picric acid (50 μL) and 0.75 mol/L sodium hydroxide solution (50 μL), followed by incubating in the 96-well microplate at 30°C for 20 min. After finishing the reaction, measure the

 doi:10.20944/preprints202211.0372.v1

absorbance of the sample at 520 nm with the blank solution as the control using SAFIRE TECAN.

2.14.4 Preparation of Tissue Homogenates and Evaluation of Oxidative Stress Markers

Rats were euthanized to death using ketamine (300 mg/kg *b.w.*) at the end of the experiment after blood samples had been collected from the animals (Shill et al., 2021). The rats' kidneys were removed and kept for later examination. 1 g of kidney tissue was homogenized in 10 mL of phosphate buffer (pH 7.4), and the kidney samples were then centrifuged at 8000 rpm for 15 min at 4 °C. For pending analysis, the supernatant was kept in a freezer at -20°C.

Nitric oxide (NO) levels and advanced oxidative protein products (AOPP) levels were identified as indicators of oxidative stress (Tracey et al., 1995)(Witko-Sarsat et al., 1996). By comparing NO to the corresponding blank solutions, we evaluated NO (absorbance measured at 540 nm). From a standard curve, the concentration of NO was estimated as nmol/g of tissue. To measure the amounts of AOPP, we used 5 µL of the sample, 95 µL of PBS, 50 µL of acetic acid, and 2 minutes of incubation. At 340 nm, the measurement was taken. Using PBS (100 µL), 50 µL acetic acid, and potassium iodide, the blank reading was measured. Finally, using the chloramine-T linear chart at 340 nm (with chloramine-T concentrations ranging from 0 to 100 nmol/mL), we computed the AOPP levels (Shill et al., 2021).

2.14.5 Study of Antioxidant Activities

Both reduced glutathione (GSH) and superoxide dismutase (SOD) are strong antioxidant enzymes. In order to determine the SOD activity in kidney tissue homogenates, we used the proven techniques (Misra & Fridovich, 1972; Shill et al., 2021). After a short interval, we filled the 96-well plates with 90 µL PBS, 10 mL tissue supernatants, and 100 µL epinephrine.

Preprints (www.preprints.org) | NOT PEER-REVIEWED | Posted: 21 November 2022 doi:10.20944/preprints202211.0372.v1

In order to calculate differences, we measured optical density (OD) at 480 nm during various time periods. A blank solution lacking of the enzyme but including all other components. In order to determine the GSH levels, we mixed 10 µL of tissue homogenate with 90 µL of PBS and 100 µL of DTNB. We then measured the absorbance at 412 nm as soon as a yellow color appeared (Jollow et al., 1974; Shill et al., 2021).

2.14.6 Histopathology Procedure

The tissue blocks were dehydrated in ascending concentrations of ethyl alcohol after being fixed in 10% formalin overnight. After that, tissues were given a xylene treatment, paraffin-embedded, and sectioned at a thickness of 5µ. Sections on slides were deparaffinized with xylene before tissues were rehydrated in alcohol at varying concentrations, from high to low. Later, hematoxylin and Sirius Red were used to stain tissue sections. Finally, stained slides were washed in xylene, mounted, viewed using an Olympus DP12 light microscope (Japan) at 20X magnification

2.15 Data analysis

The mean and standard deviation (S.D.) are used to represent all data. The graphs were created with Graphpad Prism 8.0. (GraphPad Software, LaJolla, CA). With pairwise comparisons utilizing Fisher's least significant difference method, a one-way analysis of variance was employed for statistical comparisons. In each analysis, a *p*-value of 0.05 or less was regarded as significant.

 doi:10.20944/preprints202211.0372.v1

3. Result and Discussion

In the new era of formulation development and drug delivery of limited water soluble drugs, SMSD has emerged as a promising strategy for combating the challenges of poor dissolution and bioavailability. SMSDs offer various advantages over typical SDs; including dosage reduction, consistent therapeutic efficacy, less side effects, and the ability to use a lower dose while enhancing therapeutic effectiveness (Tran et al., 2011). SMSDs usually consist of a carrier and the active pharmaceutical ingredient (API). Choosing the right carrier is important for obtaining the best drug release and therapeutic results (Tran et al., 2011). Several studies have demonstrated that the synergistic impact of polymers may result in both head-to-head and electrostatic interactions (Prasad et al., 2014). This is due to the hydrophilic groups linked to the surface by cohesive forces, which lower surface tension, resulting in the formation of an inner hydrophobic core and enhanced solubility (Bernabeu et al., 2016; R.S. et al., 2016; Raffin et al., 2010). Therefore, the current study focuses to use amphiphilic carrier in the preparation and characterization of SMSD-TQM to improve biopharmaceutical properties.

3.1 Selection of a suitable Polymer for SMSD System

A critical step in improving the biopharmaceutical properties of poorly water-soluble drugs in the SMSD system is the selection of appropriate polymers as a carrier. Amphiphilic polymers, which feature both a hydrophilic and a lipophilic unit in their structure, are gaining popularity as pharmaceutical excipients now a days. Interactions between poorly soluble pharmaceuticals and lipophilic units of amphiphilic polymers can lead to the development of polymeric micelles with a hydrophobic core and a hydrophilic shell, which can help improve the solubility of poorly water-soluble medications by encapsulation (Ahmad et al., 2014).

Preprints (www.preprints.org) | NOT PEER-REVIEWED | Posted: 21 November 2022 doi:10.20944/preprints202211.0372.v1

The apparent solubility of TQM in water was tested in the presence of several concentrations of pre-dissolved polymers such as Soluplus®, Kolliphor® P188, and Kolliphor® P407 ranging from 2 to 25 mg/mL in the present study for the selection of suitable polymers in the SMSD system for TQM. Because of their commercial availability and biocompatibility; Soluplus®, Kolliphor® P188, and Kolliphor® P407 are commonly utilized as pharmaceutical excipients with amphiphilic characteristics to increase the solubility of poorly water-soluble medicines (Gangarde et al., 2020; Ilie et al., 2021; Vasconcelos et al., 2017). Poorly water-soluble drugs can become more soluble through encapsulation owing to interactions between lipophilic units of amphiphilic polymers and poorly water-soluble drugs. These interactions can lead to the development of polymeric micelles with a hydrophobic core and a hydrophilic shell (Onoue et al., 2013) . As shown in Fig. 1, a rise in the aqueous solubility of TQM was detected when the polymer concentration increased. There was a linear association (A_L-type) between increased TQM solubility and increasing polymer concentration in all of the studied polymers. The improvement of TQM solubility by Soluplus® and Kolliphor® P407 were statistically significant (p<0.01) when compared to Kolliphor® P188. Soluplus® and Kolliphor® P407; at a concentration of 25 mg/mL, improved the aqueous solubility of TQM by 4.2 and 5.6-fold, respectively, whereas Kolliphor® P188, at the same concentration, improved it by 2.8 times. The higher dispersibility and miscibility of TQM dispersed in the polymers resulted in increased apparent solubility of TQM with amphiphilic block copolymers (Ghezzi et al., 2021; Pereira et al., 2013). Moreover, the stability constants (K_s) were determined using a linear regression analysis of the phase solubility diagram produced and the data are presented in Table 1.

The Ks is significantly higher for Soluplus® compared to Kolliphor® P407 and Kolliphor® P188; justifying the positive effect towards solubility enhancement of TQM. These findings suggested that TQM could interact better with Soluplus®; and become

Preprints (www.preprints.org) | NOT PEER-REVIEWED | Posted: 21 November 2022 doi:10.20944/preprints202211.0372.v1

entrapped in the micelle's hydrophobic core; thereby improve the solubility higher. The non-ionic polymer Soluplus® (polyvinyl caprolactam, polyvinyl acetate, polyethylene glycol) has been used extensively in the development of solubilized formulations of poorly soluble drugs, and there have been numerous reports on Soluplus®-based formulations prepared with a wide range of pharmaceutical technologies, including solid dispersion(Ha et al., 2014; Lee et al., 2015; Lin et al., 2015; Xia et al., 2016) and nanosuspensions (K. Zhang et al., 2013), resulting in improved dissolution behavior and the oral bioavailability of drugs. Therefore, based on the apparent solubility and kinetic data, Soluplus® was chosen as the carrier for the development of SMSD-TQM to improve the physicochemical behavior of TQM.

3.2 Optimization of TQM Loading Amounts by Means of Dissolution Studies

The solubilization efficiency of the target drug may be affected by the Drug loading of the SMSD formulation, perhaps because of the effectiveness of encapsulating the drug in micelle-like structures (Onoue, Suzuki, et al., 2014a). The aim of this research was to determine the optimal loading for SMSD-TQM, therefore several loadings (from 5% to 15%) were prepared using solvent evaporation by RVD and then carried through dissolution experiments in water for 60 minutes. According to the results of the dissolution tests, after 60 minutes of mixing, crystalline TQM showed only 45% drug dissolution (Table 2). To the contrary, compared to crystalline TQM and other formulations with larger loading amounts, SMSD-TQM with a drug loading of 10% (SMSD-TQM/10) showed a significant improvement in the dissolution behavior of TQM. The SMSD-TQM/10 formulation had the highest amount of TQM dissolved in the dissolution medium, followed by the SMSD-TQM/5 formulation, and finally the SMSD-TQM/15 formulation. Also, the initial dissolution rates in SMSD-TQM/5, SMSD-TQM/10, and SMSD-TQM/15 were determined to be 1.12, 1.06, and 0.77 h^{-1}. TQM's (high) affinity for the hydrophobic moiety of Soluplus®, as well as the effect

Preprints (www.preprints.org) | NOT PEER-REVIEWED | Posted: 21 November 2022 doi:10.20944/preprints202211.0372.v1

of polymer concentrations, are thought to be major contributors to the projected dissolution behavior difference (Batrakova & Kabanov, 2008). A larger Soluplus® to TQM ratio may also improve TQM encapsulation inside the micelles, leading to enhanced dispersibility in water and a subsequent acceleration of TQM solubilization. As an outcome of these findings, a 10% drug loading was selected as the preliminary step for the SMSD-TQM formulation, and its physicochemical and pharmacokinetic properties were investigated.

3.3 Physicochemical Characterizations

Because of the higher energy state, amorphous forms can have higher solubility and dissolution rates than crystalline states. As a result, determining crystallinity is critical for determining product quality. XRPD and DSC studies were used to assess the crystalline state of SMSD-TQM (Fig. 2). The XRPD pattern of crystalline TQM revealed several sharp peaks, with the strongest peak at around 20.18°, indicating the crystalline condition of TQM (Fig. 2A). SMSD-TQM/RVD and SMSD-TQM/FD; on the other hand, showed a halo diffractive pattern, and the peaks detected as in crystalline TQM were minimal in the diffractogram, indicating that TQM was in an amorphous condition. In DSC analysis, although crystalline TQM had a particular endothermic peak around 47°C corresponds to the melting point of TQM (Fig. 2B), hence the endothermic peak in SMSD-TQM/RVD and SMSD-TQM/FD at the melting point of crystalline TQM was lost in DSC analysis.

According to PLM images, crystalline TQM has a rough block-like structure (Fig. 3A-I), SMSD-TQM/RVD has small birefringence (Fig. 3A-II), and SMSD-TQM/FD has loss of polarization, which could be indicative of inner TQM in the form of an amorphous state as evidenced by negligible birefringence (Fig. 3A-III). Polarization in PLM observations can indicate a crystalline material (Li & Zhu, 2015), hence the lack of polarization in SMSD-TQM could indicate an amorphous condition of TQM in SMSD. The high free energy in the

 doi:10.20944/preprints202211.0372.v1

amorphous state may trap the drug molecule in SMSD and inhibit drug precipitation or recrystallization in the supersaturated state, which would be beneficial to improving the dissolving behavior of lipophilic drugs (Onoue, Suzuki, et al., 2014b). According to PLM, XRPD, and DSC investigations, the amorphization of DMP during the preparation procedure led to superior dissolving behavior.

The surface morphology of the TQM samples was assessed using SEM observations (Fig. 3). The morphology of crystalline TQM was irregular shaped particles and predominantly dispersed (Fig. 3B-I). On the other hand, SMSD-TQM/RVD and SMSD-TQM/FD had the appearance of typical and flaky (Fig. 3B-II and III). In comparison to the crystalline TQM, SMSD-TQM had homogenous particles, and the particle size was reduced significantly. TQM was found to be well-integrated into the polymer, implying that it was well-absorbed. In comparison to crystalline TQM, SEM micrographs clearly show that after the freeze-drying process, the surface area of pharmacological components increased significantly (Fig. 3B-III). The increased surface area obtained by micronization of particles, according to the Noyes-Whitney equation, is a significant factor for improving the dissolving rate. On the other hand, the size distribution of polymeric micelles is thought to be one of the most important elements in improving a drug's biopharmaceutical characteristics (Ghezzi et al., 2021). DLS analysis was used to examine the micellization capabilities of SMSD-TQM in this work. DLS examination of water-dispersed SMSD-TQM samples (Fig. 4) revealed the creation of uniformly nano-sized particles with a mean particle size of 68 nm for SMSD-TQM/FD with a PDI of 0.125 (Fig. 4, red line); and 145 nm with a PDI of 0.392 for SMSD-TQM/RVD (Fig. 4, blue line), respectively. Furthermore, due to their high drug solubility and increased dispersibility and diffusivity in the mucus layer by the hydrophilic chain on the surface of polymeric micelles, their size of 150 nm would aid rapid drug absorption after oral administration (Ki et al., 2004).

 doi:10.20944/preprints202211.0372.v1

Therefore, the absence of crystalline TQM throughout the SMSD-TQM preparation process was confirmed by SEM pictures and DLS data. These benefits may contribute to TQM's better dissolution behavior.

3.4 Dissolution Behavior of the Optimized Formulation in Comparing the Effect of Drying in the Preparation of SMSD-TQM

Since solubility is a key issue with crystalline TQM in therapeutic applications, *in vitro* dissolution tests were performed to determine whether the rate and total amount of drug release from various formulations were improved and to predict the drug release profile inside the physiological environment as well. , are used to determine (Bai et al., 2011). Dissolution investigations on TQM samples were conducted in water to see if different drying processes improved the dissolution behavior of SMSD-TQM, as shown in Fig. 5. The amount of TQM dissolved in 60 minutes was 0.45 mg/mL with a dissolution rate constant of 0.767 indicating crystalline TQM possessed a limited dissolution characteristics. In contrast, the dissolution behaviors of TQM in SMSD-TQM/RVD and SMSD-TQM/FD were significantly improved with complete dissolution of TQM were observed within 60 min with dissolution rate constant of 1.06 and 1.46, respectively. No traces of precipitation or agglomeration of dissolved substances was observed. The findings were in corroboration with previous studies, which showed that by increasing the surface area of the particles and by decreasing diffusion layer thickness as a result of pulverization can enhance dissolution rate proportionally (Dokoumetzidis & Macheras, 2006). Due to the uniform distribution of the active components in an amphiphilic carrier, the SMSD method can increase wettability and dispersibility of poorly water-soluble drugs (Sareen et al., 2012). During the manufacturing process, TQM and the carrier polymers were entirely dissolved in the organic solvent which may have resulted in the dissemination of TQM at a molecular level inside the SMSD system,

Preprints (www.preprints.org) | NOT PEER-REVIEWED | Posted: 21 November 2022 doi:10.20944/preprints202211.0372.v1

leading to the fast dissolution and dispersion of TQM molecules in the dissolution media. Based on these findings, it can be suggested that the dissolution time and amount of SMSD-TQM were improved compared to the crystalline TQM which may attribute to an increased TQM oral absorption.

3.5 Drug Polymer Interactions

Theoretically, amorphous molecules are molecularly disseminated in the matrix carrier in an SD formulation, and the interaction between these molecules can lead to improved drug amorphization (Onoue et al., 2012). The molecular state of crystalline TQM and processed SMSD-TQM was assessed using FT-IR analysis (Fig 6). The distinctive strong stretching band of the carbonyl group was observed at wavenumber 1652.38 cm^{-1} while at 2967.13 cm^{-1} C-H stretching of the aliphatic groups is represented by a strong band. The stretching in the vinylic C-H in the C=C-H groups was attributed to the weaker band seen at a higher wavenumber (3254.68 cm^{-1}). At 1612.32 cm^{-1}, the C=C stretching produced a unique, moderately strong band. The strong carboxylic stretching band in TQM present in this frequency range clearly depicts the C=C stretching. Furthermore, the C=C stretching, which lacks methyl and isopropyl substituents, is predicted to have a lower intensity than the carboxylic band. In contrast, Soluplus® showed peaks at 3458.9 cm^{-1} (O–H stretching), 2924.21 cm^{-1} (aromatic C–H stretching), 1732.49 cm^{-1}, 1632.35 cm^{-1} (C=O stretching), and 1440.64 cm^{-1} (C–O–C stretching) (Fig. 6A–III).

The absence of a distinctive peak in the IR spectra of the SMSD-TQM/RVD and SMSD-TQM/FD indicates negligible interaction. It is a clear indication that maximum amount of TQM was encapsulated in the core of SMSD-TQM although a little amount of TQM may be present on the surface of the nanoparticles. TQM-amount was insignificant to be detected in comparison of SMSD-TQM which supports the absence of any significant

Preprints (www.preprints.org) | NOT PEER-REVIEWED | Posted: 21 November 2022 doi:10.20944/preprints202211.0372.v1

chemical interactions between TQM and Soluplus® during the preparation. From a theoretical aspect, this is desirable since some drug-polymer interactions may actually slow down the dissolution process, and the thermodynamic driving force for dissolution will be stronger if the drug-polymer interactions are weak or non-existent (Boonsongrit et al., 2008; Pandey et al., 2015).

3.6 Pharmacokinetic Profiling

The potential improvement in absorption of TQM through SMSD formulation strategy was demonstrated by pharmacokinetic studies carried out in rats after oral administration of crystalline TQM (10 mg/kg, suspended in 0.25 % CMC suspension) and SMSD-TQM (5 mg-TQM/kg, dispersed in water) (Fig. 7). Values of the relevant pharmacokinetic parameters including C_{max}, T_{max}, $t_{1/2}$, $AUC_{0-\infty}$, and oral BA are listed in Table 3. Oral administration of crystalline TQM exhibited poor systemic absorption with a C_{max} value 165.5±23.3 ng/mL, and AUC_{0-6} 488.1 ± 89.7 ng*h/mL. In contrast, the pharmacokinetic behavior of SMSD-TQM/RVD and SMSD-TQM/FD were better than that of crystalline TQM as shown by a rapid elevation of C_{max} value of 298.2 ± 32.6 and 425.1 ± 11.2 ng/mL respectively with AUC_{0-6} of 1,002.5 ± 122.3 and 1,049.3 ± 44.44 ng*h/mL respectively.

On the basis of the $AUC_{0-\infty}$ value of intravenously administered TQM (1 mg/kg), absolute bioavailabilities of crystalline TQM, SMSD-TQM/RVD, and SMSD-TQM/FD were calculated to be 2.8%, 12.5%, and 13.7%, respectively. Thus compared to crystalline TQM an approximately 4.5 and 4.9-fold enhancement in plasma concentration were achieved with SMSD-TQM/RVD, and SMSD-TQM/FD respectively and this could be in agreement with dissolution characteristics. It was hypothesized that the faster dissolution rate of SMSD-TQM compared to crystalline TQM would lead to a shorter T_{max}, but no such difference was observed; the reason for this is still unknown, and further investigation into the absorption

 doi:10.20944/preprints202211.0372.v1

mechanism of micellar TQM is required before a plausible hypothesis can be proposed (Morgen et al., 2012).

TQM is categorized and identified as exhibiting poor aqueous solubility. For this type of compounds, absorption is limited by its dissolution rate, and a small increase in dissolution rate may lead to marked improvement in absorption characteristics (Kohli et al., 2010). The dissolution behavior and biopharmaceutical characteristics of poorly water-soluble compounds may be improved by exploiting the micellizing property of amphiphilic polymers in SMSD formulation (Kawabata et al., 2011; Onoue, Suzuki, et al., 2014b). A higher ratio of soluplus may help to stabilize TQM under gastrointestinal circumstances by encapsulating it within the micelles of soluplus, which may have contributed to the enhanced oral absorption of TQM in the current study (Kojo et al., 2017b; Shi et al., 2017). Soluplus, as seen in the dissolution tests, demonstrated better solubilization capacity to accomplish quick dissolution and maintain supersaturation that can inhibit recrystallization, potentially leading to a large enhancement of oral bioavailability by the spring and parachute effect (Banik et al., 2022; Halder et al., 2019).

3.7 Nephroprotective Effect of TQM Samples in Cisplatin-treated Rats

Our evaluation of TQM's nephroprotective effect was prompted by the increase in oral absorption in SMSD-TQM. In a rat model of nephropathy induced by cisplatin, the nephroprotective impact of TQM samples was assessed in a cisplatin-induced rat model of nephropathy using BUN and creatinine levels as biomarkers of the disease. The BUN and creatinine levels of the vehicle group increased significantly by cisplatin treatment, which resulted in nephropathy (Fig. 8). Oral doses of SMSD-TQM significantly reduced the elevated levels of BUN and creatinine values when compared to that of the vehicle group. The suppression rates of these elevations were estimated to be approximately 42% and 56%

 doi:10.20944/preprints202211.0372.v1

for creatinine and 57.3% and 63.2% for BUN for SMSD-TQM/RVD and SMSD-TQM/FD, respectively (Fig. 8). While crystalline TQM likewise prevented an increase in BUN and creatinine levels by around 26% and 28%, respectively, SMSD-TQM tended to do so more so than crystalline TQM (Fig. 8). In addition, the oxidative stress was also measured by determining the NO and AOPP levels in the kidney homogenates. This study demonstrated that intraperitoneal administration of cisplatin significantly increased NO and AOPP levels in the experimental rats which were discernibly lowered by the oral gavage of the drugs(TQM and SMSD-TQM) (Fig. 8). Since GSH and SOD are the natural cellular antioxidants, we wanted to measure the levels of GSH and SOD to determine the capacity of the drugs to improve kidney impairment in rat models. After cisplatin administration, the levels of both GSH and SOD were profoundly decreased in the rats (Fig. 8) which were significantly improved by the oral gavage of TQM and SMSD-TQM in the disease model rats. In our study we found better effects of SMSD-TQM/FD for the improvement of antioxidant enzymes in the experimental animals (Fig. 8).

The anti-cancer drug cisplatin is frequently employed as an inducer for creating a rat model of nephropathy (Choie et al., 1981). Exposure to cisplatin leads to rapid and acute renal impairment by various mechanisms. Due to the organic cation transporter, cisplatin is preferentially taken up by the proximal tubule in the kidney, activates apoptosis through the production of ROS and causes inflammation, calcium overload, and phospholipase activation, resulting in mitochondrial malfunction and DNA damage (Marullo et al., 2013; Soni et al., 2018). TQM possesses beneficial anti-oxidant and anti-apoptotic effects, can function against nephropathy and hence likely to provide a nephroprotective effect (Farooqui et al., 2017). (Dera et al., 2020; Lutfi et al., 2021). In this study, we have shown that the solubility and oral absorption of SMSD-TQM were significantly improved when compared to the crystalline TQM suggesting superior nephroprotective efficacy of the formulations.

Preprints (www.preprints.org) | NOT PEER-REVIEWED | Posted: 21 November 2022 doi:10.20944/preprints202211.0372.v1

3.8 Histopathological Assessment

Histological examination of the kidneys exposed to cisplatin showed a distinctive pattern exhibiting degeneration of tubular architecture and infiltration of inflammatory cells not observed in control renal tissue sections (Figure 9A &9B). Administration of cisplatin increased fibrotic tissue and collagen deposition in renal tissue compared to the control group (Fig. 9B). Interestingly, this morphological alteration was reversed by administration of TQM samples (crystalline TQM, SMSD-TQM/RVD, and SMSD-TQM/FD) at all doses (Fig. 9C to 9E). Furthermore, the increase in percent of collagen content in cisplatin group was significantly higher compared to that of the control group (Fig. 9A) and administration of TQM reduced the collagen content in renal tissue in a dose-dependent manner (Fig. 9). For further pharmacological characterization, it would be worth employing an appropriate animal model of chronic renal injury or fibrosis, and to investigate the effect of the SMSD-TQM formulations through *in vivo* study which may provide further insight into the therapeutic potential of SMSD-TQM in the treatment of renal dysfunction and fibrosis.

 doi:10.20944/preprints202211.0372.v1

4. Conclusion

For the purpose of improving the physicochemical and biopharmaceutical properties, a TQM-loaded SMSD formulation was developed. The optimized SMSD-TQM formulation significantly accelerated dissolution behavior micellization. The pharmacokinetic result reveals that TQM is well absorbed orally. Because of its ability to reduce oxidative stress, SMSD-TQM has been shown in this study to have more antifibrotic effects than crystalline TQM. Thus, the TQM-loaded SMSD formulation may be a viable carrier for delivering TQM for enhanced oral bioavailability and nutraceutical properties.

Conflict of Interests

The authors confirm that they have no known financial or interpersonal conflicts that would have appeared to have an impact on the study findings of this research.

Acknowledgements

This work was supported in part by a research grant from the University of Dhaka (Centennial Research Grant/Reg./Admin-3/47868, 2020-2021). The authors also wish to thank the authority of the Semiconductor Research Center, University of Dhaka for their kindness in permitting the particle size analysis of the samples. The authors also thanks the University of Dhaka for supporting the Open Access Publication charges.

 doi:10.20944/preprints202211.0372.v1

References

Ahmad, Z., Shah, A., Siddiq, M., & Kraatz, H.-B. (2014). Polymeric micelles as drug delivery vehicles. *RSC Advances*, *4*(33), 141–170. https://doi.org/10.1039/C3RA47370H

Alam, M. A., Ali, R., Al-Jenoobi, F. I., & Al-Mohizea, A. M. (2012). Solid dispersions: a strategy for poorly aqueous soluble drugs and technology updates. *Expert Opinion on Drug Delivery*, *9*(11), 1419–1440. https://doi.org/10.1517/17425247.2012.732064

Bai, G., Wang, Y., & Armenante, P. M. (2011). Velocity profiles and shear strain rate variability in the USP Dissolution Testing Apparatus 2 at different impeller agitation speeds. *International Journal of Pharmaceutics*, *403*(1–2), 1–14. https://doi.org/10.1016/j.ijpharm.2010.09.022

Banik, S., & Ghosh, A. (2021). Prevalence of chronic kidney disease in Bangladesh: a systematic review and meta-analysis. *International Urology and Nephrology*, *53*(4), 713–718. https://doi.org/10.1007/s11255-020-02597-6

Banik, S., Sato, H., & Onoue, S. (2022). Self-micellizing solid dispersion of atorvastatin with improved physicochemical stability and oral absorption. *Journal of Drug Delivery Science and Technology*, *68*(August 2021), 103065. https://doi.org/10.1016/j.jddst.2021.103065

Batrakova, E. V, & Kabanov, A. V. (2008). Pluronic block copolymers: Evolution of drug delivery concept from inert nanocarriers to biological response modifiers. *Journal of Controlled Release*, *130*(2), 98–106. https://doi.org/https://doi.org/10.1016/j.jconrel.2008.04.013

Benzoate, E. (2019). *Application of Solid Dispersion Technique to*. 1–18.

Bernabeu, E., Gonzalez, L., Cagel, M., Gergic, E. P., Moretton, M. A., & Chiappetta, D. A. (2016). Novel Soluplus®-TPGS mixed micelles for encapsulation of paclitaxel with enhanced in vitro cytotoxicity on breast and ovarian cancer cell lines. *Colloids and*

Surfaces B: Biointerfaces, *140*, 403–411. https://doi.org/10.1016/j.colsurfb.2016.01.003

Boonsongrit, Y., Mueller, B. W., & Mitrevej, A. (2008). Characterization of drug-chitosan interaction by 1H NMR, FTIR and isothermal titration calorimetry. *European Journal of Pharmaceutics and Biopharmaceutics*, *69*(1), 388–395. https://doi.org/10.1016/j.ejpb.2007.11.008

Chavan, R. B., Thipparaboina, R., Kumar, D., & Shastri, N. R. (2016). Co amorphous systems: A product development perspective. *International Journal of Pharmaceutics*, *515*(1–2), 403–415. https://doi.org/10.1016/j.ijpharm.2016.10.043

Choie, D. D., Longnecker, D. S., & del Campo, A. A. (1981). Acute and chronic cisplatin nephropathy in rats. *Laboratory Investigation; a Journal of Technical Methods and Pathology*, *44*(5), 397–402.

Dera, A. A., Rajagopalan, P., Alfhili, M. A., Ahmed, I., & Chandramoorthy, H. C. (2020). Thymoquinone attenuates oxidative stress of kidney mitochondria and exerts nephroprotective effects in oxonic acid-induced hyperuricemia rats. *BioFactors*, *46*(2), 292–300. https://doi.org/10.1002/biof.1590

Dokoumetzidis, A., & Macheras, P. (2006). A century of dissolution research: From Noyes and Whitney to the Biopharmaceutics Classification System. *International Journal of Pharmaceutics*, *321*(1), 1–11. https://doi.org/https://doi.org/10.1016/j.ijpharm.2006.07.011

Elmowafy, M., Samy, A., Raslan, M. A., Salama, A., Said, R. A., Abdelaziz, A. E., El-Eraky, W., El Awdan, S., & Viitala, T. (2016). Enhancement of Bioavailability and Pharmacodynamic Effects of Thymoquinone Via Nanostructured Lipid Carrier (NLC) Formulation. *AAPS PharmSciTech*, *17*(3), 663–672. https://doi.org/10.1208/s12249-015-0391-0

Fahmy, H. M., Khardrawy, Y. A., Abd-El Daim, T. M., Elfeky, A. S., Abd Rabo, A. A.,

Mustafa, A. B., & Mostafa, I. T. (2020). Thymoquinone-encapsulated chitosan nanoparticles coated with polysorbate 80 as a novel treatment agent in a reserpine-induced depression animal model. *Physiology and Behavior*, *222*(April), 112934. https://doi.org/10.1016/j.physbeh.2020.112934

Fahr, A., & Liu, X. (2007). Drug delivery strategies for poorly water-soluble drugs. *Expert Opinion on Drug Delivery*, *4*(4), 403–416. https://doi.org/10.1517/17425247.4.4.403

Farooqui, Z., Shahid, F., Khan, A. A., & Khan, F. (2017). Oral administration of Nigella sativa oil and thymoquinone attenuates long term cisplatin treatment induced toxicity and oxidative damage in rat kidney. *Biomedicine and Pharmacotherapy*, *96*(August), 912–923. https://doi.org/10.1016/j.biopha.2017.12.007

Gangarde, Y. M., T. K., S., Panigrahi, N. R., Mishra, R. K., & Saraogi, I. (2020). Amphiphilic Small-Molecule Assemblies to Enhance the Solubility and Stability of Hydrophobic Drugs. *ACS Omega*, *5*(43), 28375–28381. https://doi.org/10.1021/acsomega.0c04395

Ghezzi, M., Pescina, S., Padula, C., Santi, P., Del Favero, E., Cantù, L., & Nicoli, S. (2021). Polymeric micelles in drug delivery: An insight of the techniques for their characterization and assessment in biorelevant conditions. *Journal of Controlled Release*, *332*, 312–336. https://doi.org/https://doi.org/10.1016/j.jconrel.2021.02.031

Goyal, S. N., Prajapati, C. P., Gore, P. R., Patil, C. R., Mahajan, U. B., Sharma, C., Talla, S. P., & Ojha, S. K. (2017). Therapeutic potential and pharmaceutical development of thymoquinone: A multitargeted molecule of natural origin. *Frontiers in Pharmacology*, *8*(SEP), 1–19. https://doi.org/10.3389/fphar.2017.00656

Ha, E., Baek, I., Cho, W., Hwang, S., & Kim, M. (2014). Preparation and evaluation of solid dispersion of atorvastatin calcium with Soluplus® by spray drying technique. *Chemical & Pharmaceutical Bulletin*, *62*(6), 545–551. https://doi.org/10.1248/cpb.c14-00030

 doi:10.20944/preprints202211.0372.v1

Halder, S., Suzuki, H., Seto, Y., Sato, H., & Onoue, S. (2019). Megestrol acetate-loaded self-micellizing solid dispersion system for improved oral absorption and reduced food effect. *Journal of Drug Delivery Science and Technology*, *49*, 586–593. https://doi.org/10.1016/j.jddst.2018.12.033

Higuchi, T and Connors, K. A. (1965). Phase Solubility Studies. *Advances in Analytical Chemistry and Instrumentation*, *4*, 117–212.

Ilie, A.-R., Griffin, B. T., Vertzoni, M., Kuentz, M., Kolakovic, R., Prudic-Paus, A., Malash, A., Bohets, H., Herman, J., & Holm, R. (2021). Exploring precipitation inhibitors to improve in vivo absorption of cinnarizine from supersaturated lipid-based drug delivery systems. *European Journal of Pharmaceutical Sciences*, *159*, 105691. https://doi.org/https://doi.org/10.1016/j.ejps.2020.105691

Jollow, D. J., Mitchell, J. R., Zampaglione, N., & Gillette, J. R. (1974). Bromobenzene-Induced Liver Necrosis. Protective Role of Glutathione and Evidence for 3,4-Bromobenzene Oxide as the Hepatotoxic Metabolite. *Pharmacology*, *11*(3), 151–169. https://doi.org/10.1159/000136485

Kawabata, Y., Wada, K., Nakatani, M., Yamada, S., & Onoue, S. (2011). Formulation design for poorly water-soluble drugs based on biopharmaceutics classification system: Basic approaches and practical applications. *International Journal of Pharmaceutics*, *420*(1), 1–10. https://doi.org/10.1016/j.ijpharm.2011.08.032

Ki, B., Soo, J., Kang, S., Young, S., & Hong, S. (2004). *Development of self-microemulsifying drug delivery systems (SMEDDS) for oral bioavailability enhancement of simvastatin in beagle dogs*. *274*, 65–73. https://doi.org/10.1016/j.ijpharm.2003.12.028

Kohli, K., Chopra, S., Dhar, D., Arora, S., & Khar, R. K. (2010). Self-emulsifying drug delivery systems: An approach to enhance oral bioavailability. In *Drug Discovery Today*

 doi:10.20944/preprints202211.0372.v1

(Vol. 15, Issues 21–22, pp. 958–965). https://doi.org/10.1016/j.drudis.2010.08.007

Kojo, Y., Matsunaga, S., Suzuki, H., Sato, H., Seto, Y., & Onoue, S. (2017a). Improved oral absorption profile of itraconazole in hypochlorhydria by self-micellizing solid dispersion approach. *European Journal of Pharmaceutical Sciences*, *97*(5), 55–61. https://doi.org/10.1016/j.ejps.2016.10.032

Kojo, Y., Matsunaga, S., Suzuki, H., Sato, H., Seto, Y., & Onoue, S. (2017b). Improved oral absorption profile of itraconazole in hypochlorhydria by self-micellizing solid dispersion approach. *European Journal of Pharmaceutical Sciences*, *97*, 55–61. https://doi.org/10.1016/j.ejps.2016.10.032

Lee, J. Y., Kang, W. S., Piao, J., Yoon, I. S., Kim, D. D., & Cho, H. J. (2015). Soluplus®/TPGSGS-based solid dispersions prepared by hot-melt extrusion equipped with twin-screw systems for enhancing oral bioavailability of valsartan. *Drug Design, Development and Therapy*, *9*, 2745–2756. https://doi.org/10.2147/DDDT.S84070

Letchford, K., & Burt, H. (2007). A review of the formation and classification of amphiphilic block copolymer nanoparticulate structures: micelles, nanospheres, nanocapsules and polymersomes. *European Journal of Pharmaceutics and Biopharmaceutics*, *65*(3), 259–269. https://doi.org/10.1016/j.ejpb.2006.11.009

Li, C., & Zhu, Y. (2015). Quantitative polarized light microscopy using spectral multiplexing interferometry. *Optics Letters*, *40*(11), 2622–2625. https://doi.org/10.1364/ol.40.002622

Lin, Q., Fu, Y., Li, J., Qu, M., Deng, L., Gong, T., & Zhang, Z. (2015). A (polyvinyl caprolactam-polyvinyl acetate-polyethylene glycol graft copolymer)-dispersed sustained-release tablet for imperialine to simultaneously prolong the drug release and improve the oral bioavailability. *European Journal of Pharmaceutical Sciences*, *79*, 44–52. https://doi.org/10.1016/j.ejps.2015.08.018

Lutfi, M. F., Abdel-Moneim, A. M. H., Alsharidah, A. S., Mobark, M. A., Abdellatif, A. A.

H., Saleem, I. Y., Rugaie, O. Al, Mohany, K. M., & Alsharidah, M. (2021). Thymoquinone lowers blood glucose and reduces oxidative stress in a rat model of diabetes. *Molecules*, *26*(8), 1–13. https://doi.org/10.3390/molecules26082348

Marullo, R., Werner, E., Degtyareva, N., Moore, B., Altavilla, G., Ramalingam, S. S., & Doetsch, P. W. (2013). Cisplatin induces a mitochondrial-ROS response that contributes to cytotoxicity depending on mitochondrial redox status and bioenergetic functions. *PloS One*, *8*(11), e81162. https://doi.org/10.1371/journal.pone.0081162

Misra, H. P., & Fridovich, I. (1972). The Role of Superoxide Anion in the Autoxidation of Epinephrine and a Simple Assay for Superoxide Dismutase. *Journal of Biological Chemistry*, *247*(10), 3170–3175. https://doi.org/https://doi.org/10.1016/S0021-9258(19)45228-9

Morgen, M., Bloom, C., Beyerinck, R., Bello, A., Song, W., Wilkinson, K., Steenwyk, R., & Shamblin, S. (2012). Polymeric Nanoparticles for Increased Oral Bioavailability and Rapid Absorption Using Celecoxib as a Model of a Low-Solubility, High-Permeability Drug. *Pharmaceutical Research*, *29*(2), 427–440. https://doi.org/10.1007/s11095-011-0558-7

Nihei, T., Sato, H., & Onoue, S. (2021). Biopharmaceutical characterization of a novel sustained-release formulation of allopurinol with reduced nephrotoxicity. *Biopharmaceutics & Drug Disposition*, *42*(2–3), 78–84. https://doi.org/https://doi.org/10.1002/bdd.2260

Noor, N. S., Kaus, N. H. M., Szewczuk, M. R., & Hamid, S. B. S. (2021). Formulation, characterization and cytotoxicity effects of novel thymoquinone-plga-pf68 nanoparticles. *International Journal of Molecular Sciences*, *22*(17). https://doi.org/10.3390/ijms22179420

Onoue, S., Kojo, Y., Aoki, Y., Kawabata, Y., Yamauchi, Y., & Yamada, S. (2012).

Physicochemical and pharmacokinetic characterization of amorphous solid dispersion of tranilast with enhanced solubility in gastric fluid and improved oral bioavailability. *Drug Metabolism and Pharmacokinetics*, *27*(4), 379–387. https://doi.org/10.2133/dmpk.DMPK-11-RG-101

Onoue, S., Kojo, Y., Suzuki, H., Yuminoki, K., Kou, K., Kawabata, Y., Yamauchi, Y., Hashimoto, N., & Yamada, S. (2013). Development of novel solid dispersion of tranilast using amphiphilic block copolymer for improved oral bioavailability. *International Journal of Pharmaceutics*, *452*(1–2), 220–226. https://doi.org/10.1016/j.ijpharm.2013.05.022

Onoue, S., Suzuki, H., Kojo, Y., Matsunaga, S., & Sato, H. (2014a). Self-micellizing solid dispersion of cyclosporine A with improved dissolution and oral bioavailability. *EUROPEAN JOURNAL OF PHARMACEUTICAL SCIENCES*, *62*, 16–22. https://doi.org/10.1016/j.ejps.2014.05.006

Onoue, S., Suzuki, H., Kojo, Y., Matsunaga, S., Sato, H., Mizumoto, T., Yuminoki, K., Hashimoto, N., & Yamada, S. (2014b). Self-micellizing solid dispersion of cyclosporine A with improved dissolution and oral bioavailability. *European Journal of Pharmaceutical Sciences*, *62*, 16–22. https://doi.org/10.1016/j.ejps.2014.05.006

Onoue, S., Yamada, S., & Chan, H. K. (2014). Nanodrugs: Pharmacokinetics and safety. In *International Journal of Nanomedicine* (Vol. 9, Issue 1, pp. 1025–1037). https://doi.org/10.2147/IJN.S38378

Pandey, M. M., Jaipal, A., Charde, S. Y., Goel, P., & Kumar, L. (2015). Dissolution enhancement of felodipine by amorphous nanodispersions using an amphiphilic polymer: insight into the role of drug–polymer interactions on drug dissolution. *Pharmaceutical Development and Technology*, *00*(00), 1–12. https://doi.org/10.3109/10837450.2015.1022785

 doi:10.20944/preprints202211.0372.v1

Pereira, J. M., Mejia-Ariza, R., Ilevbare, G. A., McGettigan, H. E., Sriranganathan, N., Taylor, L. S., Davis, R. M., & Edgar, K. J. (2013). Interplay of Degradation, Dissolution and Stabilization of Clarithromycin and Its Amorphous Solid Dispersions. *Molecular Pharmaceutics*, *10*(12), 4640–4653. https://doi.org/10.1021/mp400441d

Prasad, D., Chauhan, H., & Atef, E. (2014). Amorphous stabilization and dissolution enhancement of amorphous ternary solid dispersions: Combination of polymers showing drug-polymer interaction for synergistic effects. *Journal of Pharmaceutical Sciences*, *103*(11), 3511–3523. https://doi.org/10.1002/jps.24137

R.S., B., A.S., J., D.T., M., A.G., J., P.A., R. H., & M.S., N. (2016). Soluplus based polymeric micelles and mixed micelles of lornoxicam: Design, characterization and In vivo efficacy studies in rats. *Indian Journal of Pharmaceutical Education and Research*, *50*(2), 277–286. https://doi.org/10.5530/ijper.50.2.8

Raffin, R. P., Colomé, L. M., Hoffmeister, C. R. D., Colombo, P., Rossi, A., Sonvico, F., Colomé, L. M., Natalini, C. C., Pohlmann, A. R., Costa, T. D., & Guterres, S. S. (2010). Pharmacokinetics evaluation of soft agglomerates for prompt delivery of enteric pantoprazole-loaded microparticles. *European Journal of Pharmaceutics and Biopharmaceutics*, *74*(2), 275–280. https://doi.org/10.1016/j.ejpb.2009.11.015

Sampson, E. J., & Baird, M. A. (1979). Chemical inhibition used in a kinetic urease/glutamate dehydrogenase method for urea in serum. *Clinical Chemistry*, *25*(10), 1721–1729. https://doi.org/10.1093/clinchem/25.10.1721

Sareen, S., Joseph, L., & Mathew, G. (2012). Improvement in solubility of poor water-soluble drugs by solid dispersion. *International Journal of Pharmaceutical Investigation*, *2*(1), 12. https://doi.org/10.4103/2230-973x.96921

Shaterzadeh-Yazdi, H., Noorbakhsh, M.-F., Samarghandian, S., & Farkhondeh, T. (2018). An Overview on Renoprotective Effects of Thymoquinone. *Kidney Diseases*, *4*(2), 74–82.

https://doi.org/10.1159/000486829

Shi, N. Q., Zhang, Y., Li, Y., Lai, H. W., Xiao, X., Feng, B., & Qi, X. R. (2017). Self-micellizing solid dispersions enhance the properties and therapeutic potential of fenofibrate: Advantages, profiles and mechanisms. *International Journal of Pharmaceutics*, *528*(1–2), 563–577. https://doi.org/10.1016/j.ijpharm.2017.06.017

Shill, M. C., Bepari, A. K., Khan, M., Tasneem, Z., Ahmed, T., Hasan, M. A., Alam, M. J., Hossain, M., Rahman, M. A., Sharker, S. M., Shahriar, M., Rahman, G. M. S., & Reza, H. M. (2021). Therapeutic potentials of colocasia affinis leaf extract for the alleviation of streptozotocin-induced diabetes and diabetic complications: In vivo and in silico-based studies. *Journal of Inflammation Research*, *14*, 443–459. https://doi.org/10.2147/JIR.S297348

Soni, H., Kaminski, D., Gangaraju, R., & Adebiyi, A. (2018). Cisplatin-induced oxidative stress stimulates renal Fas ligand shedding. *Renal Failure*, *40*(1), 314–322. https://doi.org/10.1080/0886022X.2018.1456938

Suzuki, H., Kojo, Y., Yakushiji, K., Yuminoki, K., Hashimoto, N., & Onoue, S. (2016). Strategic application of self-micellizing solid dispersion technology to respirable powder formulation of tranilast for improved therapeutic potential. *International Journal of Pharmaceutics*, *499*(1–2), 255–262. https://doi.org/10.1016/j.ijpharm.2015.12.065

Suzuki, H., Sato, H., Kojo, Y., Mizumoto, T., Yuminoki, K., Hashimoto, N., Seto, Y., & Onoue, S. (2016). Development of self-micellizing solid dispersion system employing amphipathic copolymer for the improvement of dissolution and oral bioavailability of cyclosporine A. *Asian Journal of Pharmaceutical Sciences*, *11*(1), 50–51. https://doi.org/10.1016/j.ajps.2015.10.038

Tracey, W. R., Tse, J., & Carter, G. (1995). Lipopolysaccharide-induced changes in plasma nitrite and nitrate concentrations in rats and mice: pharmacological evaluation of nitric

oxide synthase inhibitors. *The Journal of Pharmacology and Experimental Therapeutics*, *272*(3), 1011–1015.

Tran, P. H. L., Tran, T. T. D., Park, J. B., & Lee, B. J. (2011). Controlled release systems containing solid dispersions: Strategies and mechanisms. In *Pharmaceutical Research* (Vol. 28, Issue 10, pp. 2353–2378). https://doi.org/10.1007/s11095-011-0449-y

Vasconcelos, T., Marques, S., & Sarmento, B. (2017). The biopharmaceutical classification system of excipients. *Therapeutic Delivery*, *8*(2), 65–78. https://doi.org/10.4155/tde-2016-0067

Witko-Sarsat, V., Friedlander, M., Capeillère-Blandin, C., Nguyen-Khoa, T., Nguyen, A. T., Zingraff, J., Jungers, P., & Descamps-Latscha, B. (1996). Advanced oxidation protein products as a novel marker of oxidative stress in uremia. *Kidney International*, *49*(5), 1304–1313. https://doi.org/10.1038/ki.1996.186

Xia, D., Yu, H., Tao, J., Zeng, J., Zhu, Q., Zhu, C., & Gan, Y. (2016). Supersaturated polymeric micelles for oral cyclosporine A delivery: The role of Soluplus-sodium dodecyl sulfate complex. *Colloids and Surfaces B: Biointerfaces*, *141*, 301–310. https://doi.org/10.1016/j.colsurfb.2016.01.047

Zhang, K., Yu, H., Luo, Q., Yang, S., Lin, X., Zhang, Y., Tian, B., & Tang, X. (2013). Increased dissolution and oral absorption of itraconazole/Soluplus extrudate compared with itraconazole nanosuspension. *European Journal of Pharmaceutics and Biopharmaceutics*, *85*(3 PART B), 1285–1292. https://doi.org/10.1016/j.ejpb.2013.03.002

Zhang, Y., Huo, M., Zhou, J., & Xie, S. (2010). PKSolver: An add-in program for pharmacokinetic and pharmacodynamic data analysis in Microsoft Excel. *Computer Methods and Programs in Biomedicine*, *99*(3), 306–314. https://doi.org/10.1016/j.cmpb.2010.01.007

Preprints (www.preprints.org) | NOT PEER-REVIEWED | Posted: 21 November 2022 doi:10.20944/preprints202211.0372.v1

Tables

Table 1. Apparent solubility data of binary complexes of TQM with different polymers

Complex/Parameter	S_0	Slope	R^2	K_s	C.E.
TQM-Soluplus®		0.0099	0.9831	1161.5	0.010
TQM-Kolliphor® P188	0.001428	0.0037	0.9735	427.1	0.004
TQM- Kolliphor® P407		0.01	0.8441	1149.4	0.010

S_0, solubility of TQM in water; Ks, stability constant; C.E., complexation efficiency

Preprints (www.preprints.org) | NOT PEER-REVIEWED | Posted: 21 November 2022 doi:10.20944/preprints202211.0372.v1

Table 2. Dissolution properties of TQM samples.

	Composition of SMSD-TQM (w/w %)		Initial dissolution rate (hr^{-1})	% dissolved at 60 min
	TQM	Soluplus®		
Crystalline TQM	100	-	0.767 ± 0.03	45.2 ± 4.6
SMSD-TQM/5	5	95	1.128 ± 0.10	73.9 ± 6.2
SMSD-TQM/10	10	90	1.062 ± 0.21	89.3 ± 6.6
SMSD-TQM/15	15	85	0.770 ± 0.14	66.7 ± 12.6

[a] Initial dissolution rate in water.

[b] Dissolved amount of TQM in water solution at 60 min. Data presented as mean ± S.D. (n = 3).

Preprints (www.preprints.org) | NOT PEER-REVIEWED | Posted: 21 November 2022 doi:10.20944/preprints202211.0372.v1

Table 3 Pharmacokinetic parameters of TQM samples following oral administration to rats

Parameters	Crystalline TQM (10 mg/kg; *p.o.*)	SMSD-TQM/RVD (5 mg-TQM/kg; *p.o.*)	SMSD-TQM/FD (5 mg-TQM/kg; *p.o.*)
C_{max} (ng/mL)	165.5 ± 23.3	298.2 ± 32.6	425.1 ± 11.2**
T_{max} (h)	0.41 ± 0.08	0.67 ± 0.16	0.41 ± 0.08
AUC_{0-6} (ng· h/mL)	488.1 ± 89.7	1,002.5 ± 122.3	1,049.3 ± 44.44*
$AUC_{0-\infty}$ (ng· h/mL)	554.6 ± 79.6	1,230.5 ± 184.3	1,349.9 ± 262.6*
MRT (h)	2.25 ± 0.05	2.23 ± 0.03	2.08 ± 0.23
$t_{1/2}$ (h)	2.3 ± 0.36	2.34 ± 0.16	2.38 ± 0.96
K_e (h^{-1})	0.31 ± 0.04	0.29 ± 0.02	0.37 ± 0.10
BA (%)	2.8	12.5	13.7

C_{max}; maximum concentration; T_{max}; time to maximum concentration; AUC_{0-6}: area under the curve of blood concentration *vs*. time from 0 h to 6 h; $AUC_{0-\infty}$; area under the curve of blood concentration *vs*. time from 0 h to infinity; MRT: mean residence time; $t_{1/2}$: elimination half-life; and K_e: elimination rate constant. Data represents mean± S.E. of 4–6 experiments. * $P<0.05$, and ** $P<0.001$ with respect to orally-dosed crystalline TQM.

Preprints (www.preprints.org) | NOT PEER-REVIEWED | Posted: 21 November 2022 doi:10.20944/preprints202211.0372.v1

Figures

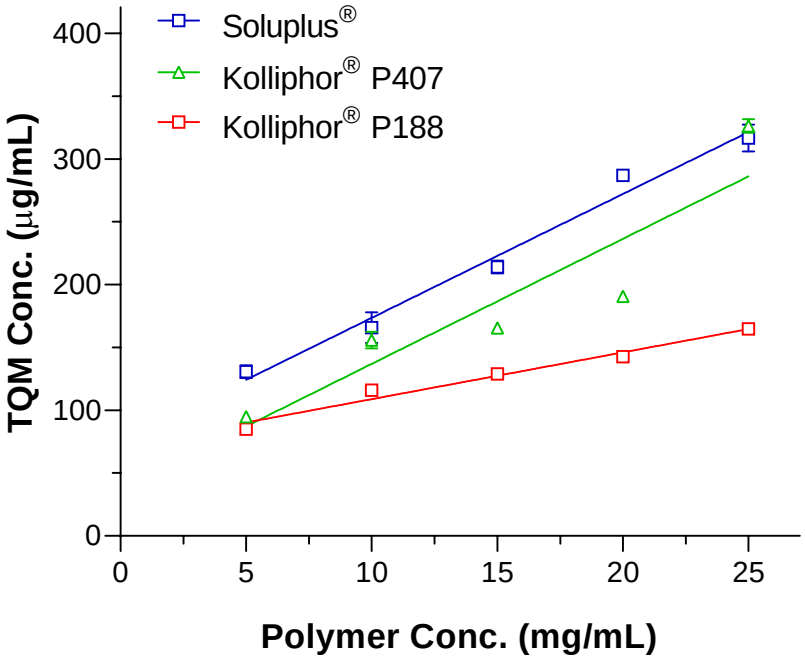

Fig. 1. Apparent solubility of TQM in aqueous solution of Soluplus®, Kolliphor® P188 and, Kolliphor® P407 at various concentrations (2–25 mg/mL). Data presented as mean ± S.D. (n = 3).

Preprints (www.preprints.org) | NOT PEER-REVIEWED | Posted: 21 November 2022 doi:10.20944/preprints202211.0372.v1

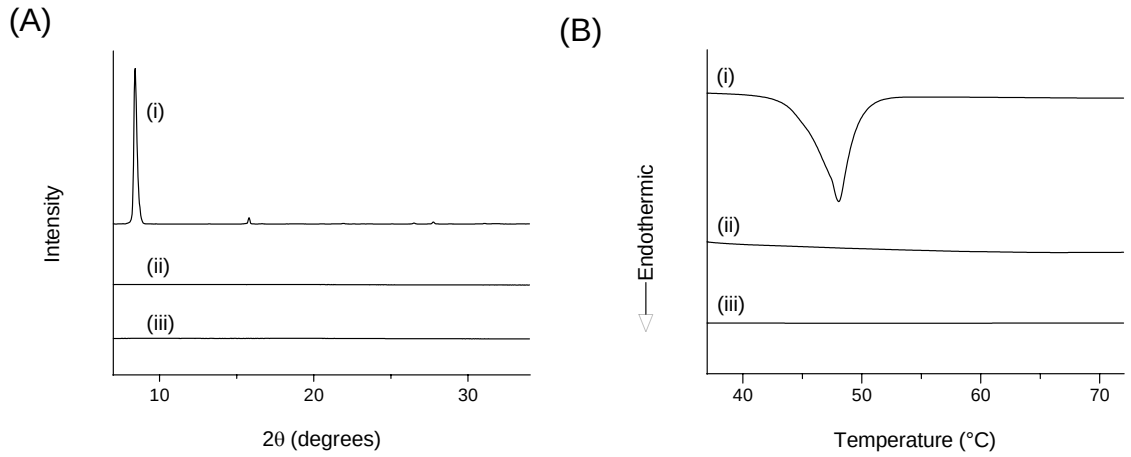

Fig. 2 Crystallinity assessment of TQM samples using (A) XRPD and (B) DSC. (I) Crystalline TQM, (II) SMSD-TQM/RVD, and (III) SMSD-TQM/FD.

Preprints (www.preprints.org) | NOT PEER-REVIEWED | Posted: 21 November 2022 doi:10.20944/preprints202211.0372.v1

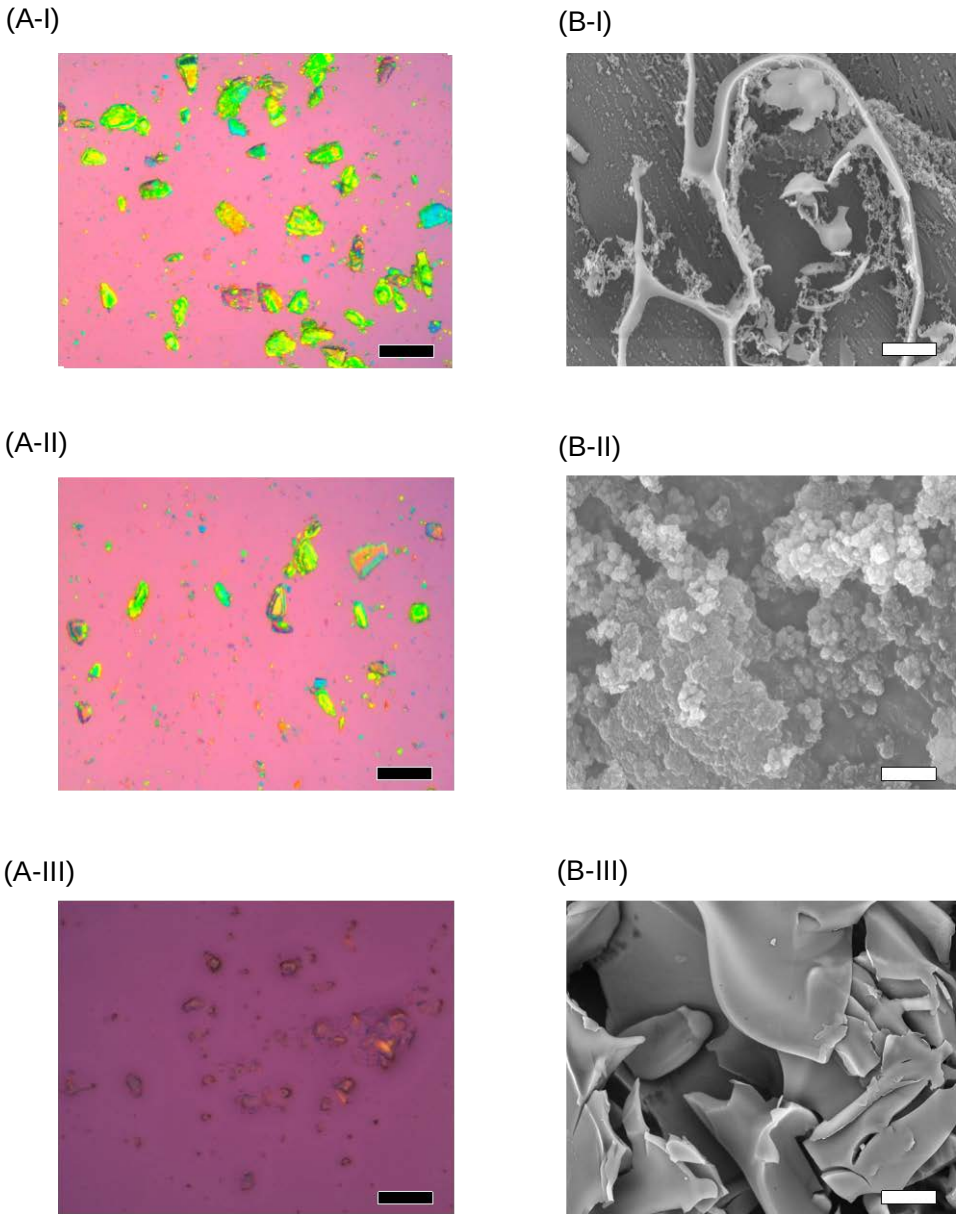

Fig. 3 Microscopic images observed by polarized light microscope (A) and scanning electron microscope (B). (I) Crystalline TQM, (II) SMSD-TQM/RVD, and (III) SMSD-TQM/FD. Each black and white bar represents 100 μm and 50 μm, respectively.

Preprints (www.preprints.org) | NOT PEER-REVIEWED | Posted: 21 November 2022 doi:10.20944/preprints202211.0372.v1

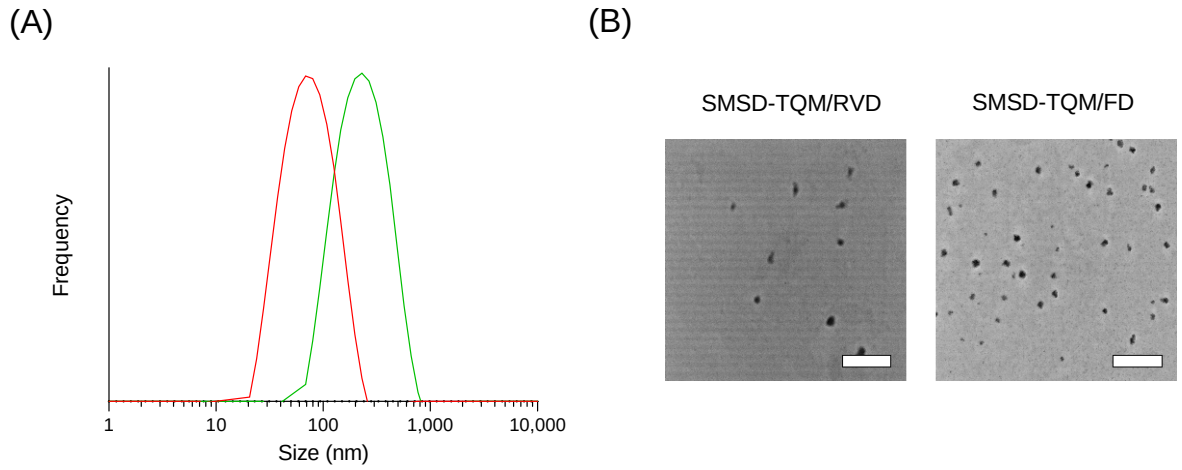

Fig. 4 Micelle forming potency of TQM samples dispersed in water. (A) Micelle size distribution of SMSD-TQM dispersed in distilled water as determined by DLS analysis: the red line represents the particle size distribution of SMSD-TQM/FD; and the blue line represents the particle size distribution of SMSD-TQM/RVD. (B) TEM image of SMSD-TQM dispersed in distilled water. Bar represents 500 nm.

Preprints (www.preprints.org) | NOT PEER-REVIEWED | Posted: 21 November 2022 doi:10.20944/preprints202211.0372.v1

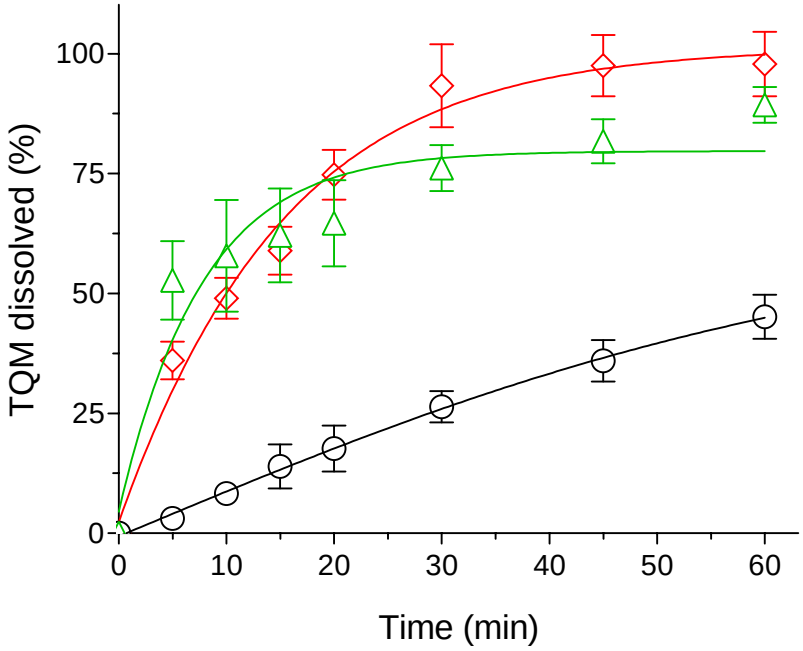

Fig. 5 Dissolution tests of TQM samples in water. ○, crystalline TQM; △, SMSD-TQM/RVD; and ◇, SMSD-TQM/FD. Data represent the mean ± S.D. of 3 experiments.

Preprints (www.preprints.org) | NOT PEER-REVIEWED | Posted: 21 November 2022 doi:10.20944/preprints202211.0372.v1

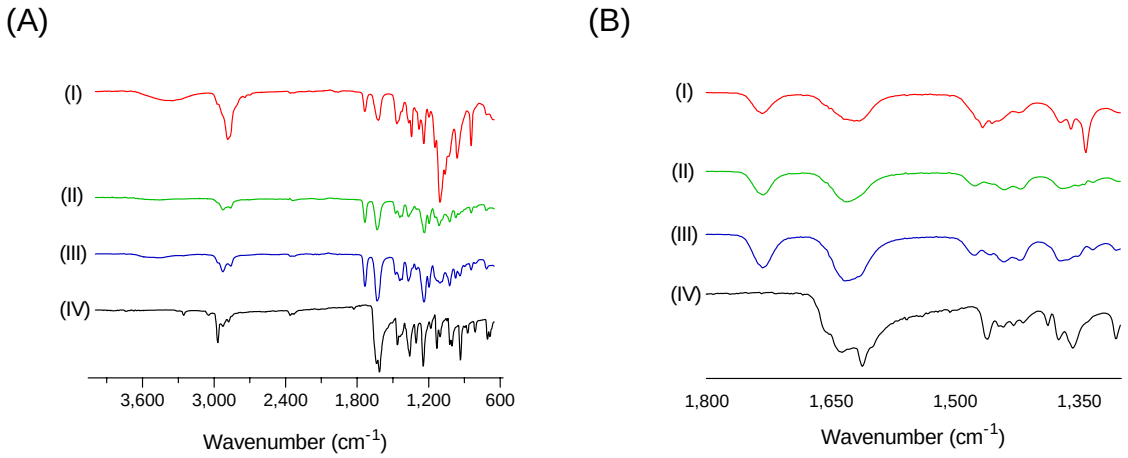

Fig. 6 Drug-polymer interaction studies of TQM samples using FT-IR. Baseline-corrected and normalized IR data of TQM samples (600–4,000 cm^{-1}). (I) SMSD-TQM/FD, (II) SMSD-TQM/RVD (III) Soluplus®, and (IV) Crystalline TQM.

Preprints (www.preprints.org) | NOT PEER-REVIEWED | Posted: 21 November 2022 doi:10.20944/preprints202211.0372.v1

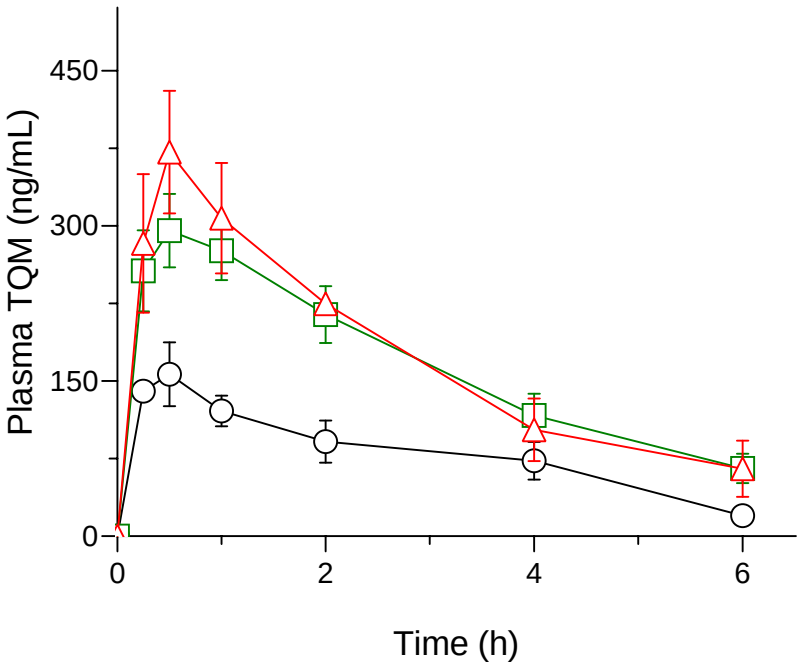

Fig. 7 Plasma concentration-time profile of TQM after oral administration of TQM samples in rats. ○, crystalline TQM (10 mg/kg, *p.o.*), □, SMSD-TQM/RVD (5 mg-TQM/kg, *p.o.*), and △, SMSD-TQM/FD (5 mg–TQM/kg, *p.o.*). Data represents mean ± S.E. of 4–6 experiments.

Preprints (www.preprints.org) | NOT PEER-REVIEWED | Posted: 21 November 2022 doi:10.20944/preprints202211.0372.v1

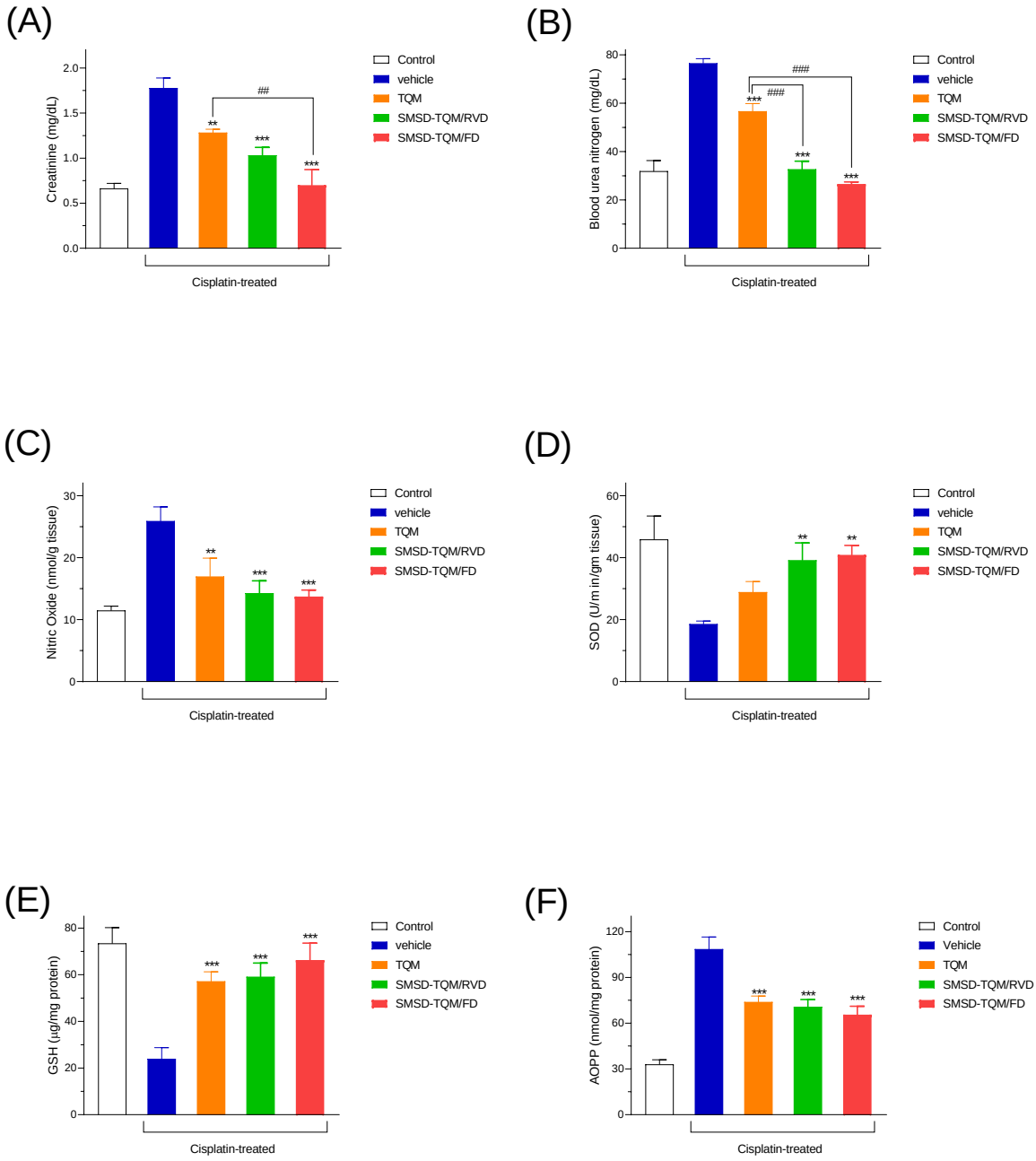

Fig. 8 Nephrotoxic potential in a rat model of nephropathy induced by cisplatin (6 mg/kg, *ip*). (A) Plasma creatinine, (B) BUN, (C) NO, (D) SOD, (E) GSH, and (F) AOPP levels in rats with orally dosed crystalline TQM and SMSD-TQM (10 mg/kg, 4 days). **, $P<0.01$; ***, $P<0.001$ with respect to cisplatin-treated rats; ##, $P<0.01$; ###, $P<0.001$, TQM *vs.* SMSD-TQM.

Preprints (www.preprints.org) | NOT PEER-REVIEWED | Posted: 21 November 2022 doi:10.20944/preprints202211.0372.v1

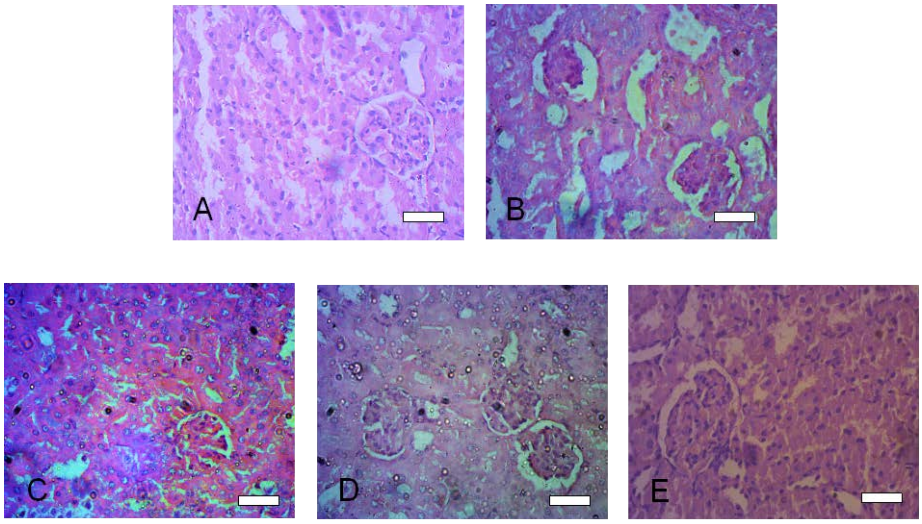

Fig. 9 Histological features of liver sections after cisplatin challenge with or without oral administration of crystalline TQM (10 mg/kg, *p.o.*) or SMSD-TQM (10 mg-TQM/kg, *p.o.*). (A) Rats treated with saline, (B) cisplatin-treated rats, (C) cisplatin-treated rats with crystalline TQM, (D) cisplatin-treated rats with SMSD-TQM/RVD and (E) cisplatin-treated rats with SMSD-TQM/FD. Each bar represents 50 µm.